Gas-Oil interaction and Gravity impact on high permeability WAG experiments.

Gilles Puyou[1], *Marcel* Bourgeois[1], *Bauyrzhan* Satken[2], *Nadine* Loubere[1], *Anthony* Chenieux[1], *Vincent* Zozaya[3], *Frederic* Merceron[1], *Nicolas* Blin[4], *Anne* Saint-Pierre[1], *Michel* Nguyen[1], *Cyril* Caubit[1], and *Yoann* Guilloux[1]

[1]TotalEnergies, CSTJF, Avenue Larribau 64018 Pau Cedex, France
[2]Akkodis, 4 Rue Jules Ferry, 64000 Pau, France
[3]SEAOWL, 3 Rue Ada Byron, 64000 Pau, France
[4]CVA, 2 rue Johannes Kepler, 64000 Pau, France

Abstract. This study evaluates the impact of the gas-oil interaction on miscible gas injection experiments, and also the gravity impact on these experiments. The program comprised 4 reservoir conditions experiments, conducted in multi-contact miscible conditions, with live oil and reservoir rock, and different WAG slug sizes, starting either with water or with gas. More conventional 2-phase laboratory condition experiments were also conducted and available for comparison. The field of interest is a high-pressure sandstone green field, in deep offshore environment, with low dip and high permeabilities.

Advanced monitoring allowed to visualize and quantify the thermodynamic phenomena of stripping and swelling for all experiments, as well as gas override and water underride for the horizontal experiments.
The results compare recovery factors, the evolution of trapped gas, water saturation, and productivity indices across various injection cycles. The experimental design allowed efficient monitoring of effluent production volumes at respective reservoir pressure and temperature conditions, and at surface conditions with clear separation of flashed oil, oil produced via gas, and gas, complemented by compositional analysis of gases and liquids.

The history match of 1D and 2D cases allowed to quantify the 2-phase petrophysical parameters like relative permeabilities, and also the three-phase parameters specific to alternate injections of gas and water (GWGW and WGWG long slugs and GWGW short slugs).

A specific focus was set on the gravity impact on a scenario with maximum gas-oil interaction (GWGW): varying the orientation from horizontal to vertical showed a substantial change in behavior: the mixing zone was much reduced, changing the nature of the gas-oil interaction.

Flow analysis and understanding were enhanced using a real time 2D X-ray imaging system to visualize 3-phase fluid distribution within the rock sample. The study's findings clearly demonstrate that alternating the phases of injection helps to stabilize and achieve better distribution of the gas, leading to enhanced recovery due to the thermodynamic exchanges.

Overall, these WAG injections illustrate the benefit of 3-phase flow even in high permeability horizontal floods: the high recovery factors, which were expected for miscible conditions, were achieved much quicker when alternating gas and water as injected phases.

1 Introduction

New policy recommends reducing or avoiding flaring in hydrocarbon production fields. However, gas export market is not always present close to production infrastructures. Two solutions can be deployed: gas storage or injection directly into the reservoir. In this second case, it is important to define the impact of a gas injection on the recovery factor and its behaviour in the reservoir.

The impact may vary depending on the context, as well as the properties of the rock and fluids involved. Bourgeois et al. [1] demonstrates that gas disposal can enable economically viable enhanced oil recovery (EOR). Pizarro et al. [2] illustrates changes in injectivity, BSW and GOR control during field operations. The variability of outcomes for WAG simulation needs anchoring on experimental data as shown by Shahverdi et al. [3]

Water alternating gas injections (WAG) were considered in this study on a high-pressure sandstone green field development. It is a deep offshore environment with low

* Corresponding author: gilles.puyou@totalenergies.com

dip and high permeability range. similar as example presented by Burns et al. [4].

The advantages of WAG injections, illustrated by Joubert et al. [5] in the WAG cross-section below (Fig. 1), in high permeability environment are expected to benefit from:

- The density differences of injection fluids (water and gas) to reach different zones of the reservoir.
- The gas / oil interaction to increase oil production under swelling and stripping effects (in zones where gas is present).

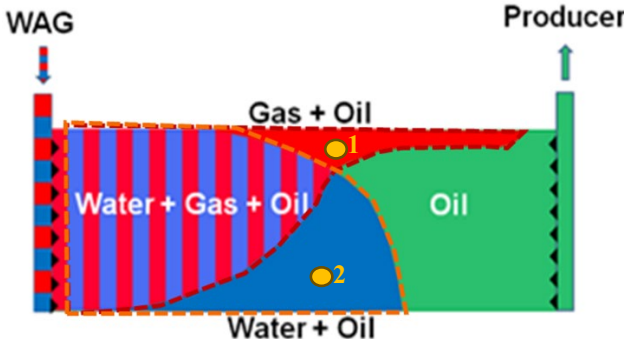

Fig. 1. Fluid path representation between two vertical wells during WAG injections

The first gas and water injections from long slug experiments in a WAG program describe flow regions respectively 1 and 2. The following slugs enabled to have information of the cycling effects and define the three-phase parameters for reservoir model simulations. Vieira et al. [6] described this link between SCAL WAG data and WAG simulations models. Short slug experiment was performed to investigate other intermediate saturation paths and evaluate the efficiency of the mechanism.

2 Core and fluid properties

2.1 Experimental conditions

Experimental conditions were set at the same level as expected reservoir condition (RC). For this program:

- Pressure was 520 bars
- Temperature was 125°C

2.2 Core sample:

The core samples used were extracted from reservoir whole cores with a diameter of 5cm. They were selected after CT-scan measurements (Fig.2) and preliminary characterisation to ensure a representative and good homogeneity of the porous medium.

Gray scale images demonstrated a homogeneous appearance across the three core samples studied. Figure 2 illustrates the perpendicular middle slices (dip and strike) along with the maximum and minimum gray scale values in the projection direction, which are essential for identifying specific objects or holes. The radio mode offers a complete projection of the core sample, when unrolled presenting the exterior surface aspect.

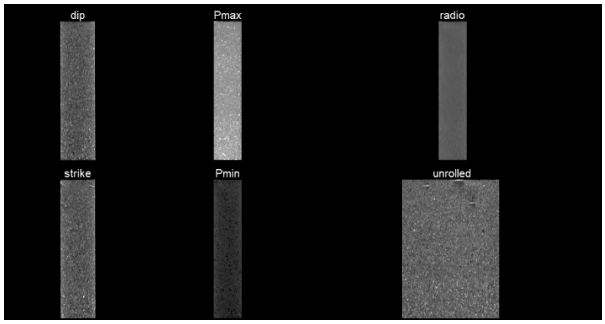

Fig. 2. Example of a CT-scan measurement on WAG2 core sample

The characteristics of the core samples are defined in - Table 1:

Table 1. Core samples characteristics

Experiments	WAG1a	WAG1b	WAG2	WAG3
Length (cm)	19.7	19.7	20.0	19.9
Diameter (cm)	5	5	5	5
Pore Volume (cc)	74.8 +/- 0.5	74.8 +/- 0.5	82.5 +/- 0.5	79.5 +/- 0.5
Porosity (%)	19.3 +/- 0.4	19.3 +/- 0.4	21 +/- 0.8	20.3 +/- 0.5
Peclet = L/α_L	210	Not measured	464	106
Kg, Kl (mD)	730 +/- 80	Not measured	1917 +/- 40	1190 +/- 240
Kw (mD)	786 +/- 6	631 +/- 6	1360 +/- 10	1273 +/- 16
Swi (%)	20.0 +/- 0.4	19.7 +/- 0.4	15.2 +/- 0.4	19.3 +/- 0.4

Same core sample was used for WAG1a and WAG1b.

It is important to note that high permeability range core samples were considered for this study. This will have a huge impact on the fluid flow paths during the WAG experiment.

2.3 Water:

The same synthetic water was used for the formation and injected water with a total salinity of 13.2 g/L. It was mainly composed of NaCl, but contained other salts such as CaCl2, MgCl2, KCl, NaHCO3 and SrCl2 (Table 2).

For the coreflood step, injected water was first equilibrated with core material and injected gas to avoid any interaction between water and gas during WAG experiment.

Table 2. Water composition

Salt	g/L
NaCl	10.846
CaCl2, 2H2O	0.235
MgCl2, 6H2O	0.058
KCl	0.109
NaHCO3	1.455
SrCl2, 6H2O	0.009
Salinity (g/L)	**13.2**

Water properties were measured by laboratory equipment tools and gave the results in Table 3.

Table 3. Water properties

Property	Value
Density (g/cc) @RC	0.969 +/- 0.002
Viscosity (cP)	0.21

2.4 Crude Oil and Live Oil

Crude oil used for experiments was directly extracted from field. After chromatography analysis of a field live oil sample, synthetic gas was added to the crude oil to retrieve Live Oil characteristics (Table 4) at reservoir conditions (P&T).

Table 4. Live oil properties

	Theoretical	Measured
Density (g/cm3) @RC	0.664	0.664 +/- 0.002
Viscosity (cP)	0.35	0.43 +/- 0.05
GOR (scc/scc)	221	217 +/- 16
Bo_i (rcc/scc)	1.61	1.603 +/- 0.14
Mw (kg/mol)	81.6	Not measured

Special attention was given to measuring the live oil viscosity using in-house capillary differential pressure measurement method, which employs Poiseuille's and Darcy's laws. This task was particularly challenging due to the high-pressure and high-temperature conditions, coupled with the low viscosity levels (below 1 cP) that needed analysis. Accurate knowledge of this value is crucial for ensuring the consistency of the permeability evolution during core preparation. As shown in Fig. 3, the following fluids were used to estimate core permeability: Water at Sw=1, and then mineral oil Marcol 52, Dead Oil (both before and after aging), and Live Oil at Swi.

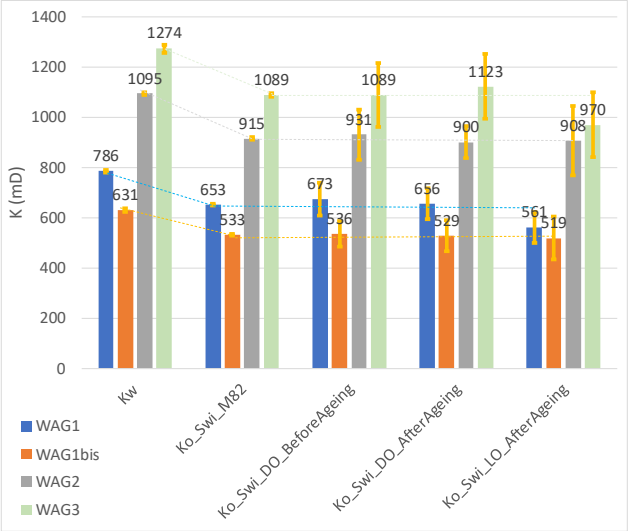

Fig. 3. Permeability estimates from viscosity

2.5 Injected gas

The injected gas is a synthetic gas created in laboratory based on the chromatography analysis (Table 5) performed on a real gas sample from the field.

Table 5. Injected gas composition from synthetic gas recombination

Component	%mol
N2	0.629
CO2	2.131
C1	78.593
C2	8.461
C3	6.177
iC4	0.948
nC4	1.832
iC5	0.417
nC5	0.359
C6	0.193
nC7	0.177
nC8	0.07
nC9	0.01
nC10	0.004
Mw, g/mol	**21.60**

Density and 1/Bg (Bg= gas formation volume factor) measurements were performed to check the validity of gas recombination. The other parameters were defined theoretically from reference equation of state (EOS). Table 6 listed all these analyses and measurements.

Table 6. Gas properties

	Theoretical	Measured
Density (g/cm3) @RC	0.293	0.297 +/- 0.002
Viscosity (cP)	0.04	-
1/Bg (scc/rcc)	333	326
Mw (g/mol)	21.5	-

2.6 Gas / oil interactions

Egerman et al. [7] demonstrated the complexity of special core analysis in presence of condensing and vaporizing gas-oil interactions. A reference EOS was defined for the simulation reservoir model. Based on this EOS, the level of interaction between gas and oil was analysed.

Bourgeois et al. [8] illustrated various levels of miscibility as described in Fig. 4 below, which we believe deserve to be differentiated.

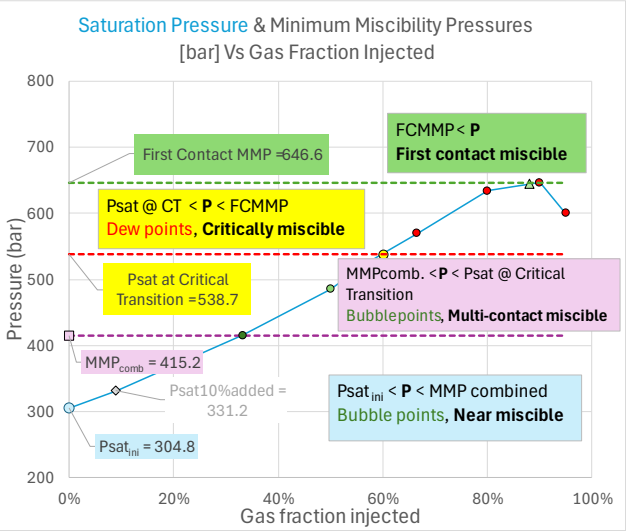

Fig.4. Saturation pressure versus gas fraction injected for reference EOS

For this study, gas-oil interaction was in the multi-contact miscible zone. In this case, when pressure is higher than MMP combined, which corresponds best to the slim tube minimum miscibility pressure. Gas-Oil relative permeability will become active a bit quicker, for low gas saturations, when the first gas bubbles appear after a lot of dissolution.

One of the most impacting parameters during coreflood experiment is the viscosity ratio between resident fluids in the porous medium and the injected fluid.

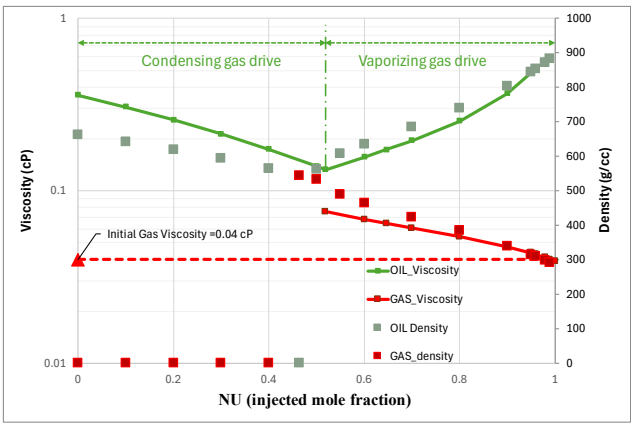

Fig. 5. Viscosity versus gas fraction injected for reference EOS

Fig.5 shows the expected changes of live oil and injected gas during the gasflood phase of the WAG experiment. A non-monotonic evolution of the oil viscosity is observed when gas exchange proportion is increasing (condensing then vaporizing gas drive). Gas viscosity is higher than the initial viscosity when gas is contacted by the oil and becomes lighter and lighter when the full exchange process is over. The initial gas viscosity is retrieved. Same behaviour is observed for the density.

3 Experimental Workflow

Duchenne et al. [9] explained that several SCAL are necessary to constrain many parameters to match, to reduce history match uncertainty and non-unicity.
This study is based on 4 reservoir conditions laboratory experiments performed to evaluate the efficiency of gasflood in the following context:

- WAG1a: long slugs horizontal injection starting by gas, then water, then gas and finally water,
- WAG1b: vertical injection with the same pattern as WAG1 to evaluate the impact of gravity,
- WAG2: long slugs horizontal injection starting by water, then gas, water and finally gas,
- WAG3: short slugs horizontal injection starting by gas and alternating water / gas injection until a final long slug injection of gas. This experiment is the most representative of the development that can be deployed on the field.

3.1 Experimental setup

The core sample is loaded into a core-holder (1 in Fig.6) and set under pressure and temperature using the confining system.

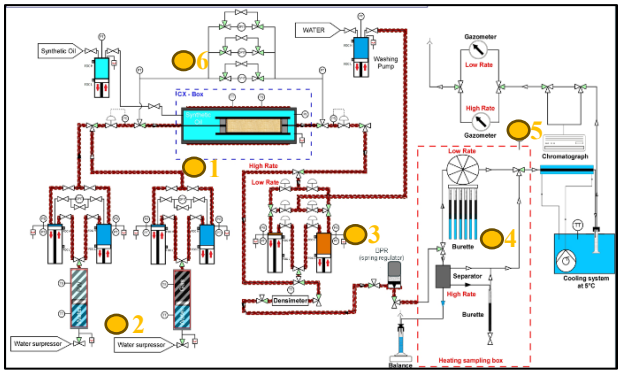

Fig. 6. Experimental setup and equipment for WAG1, WAG2 and WAG3

Two injection double-pumps (2) were connected to the inlet of the core holder and represents the injection wells for the process. They were supplied by injection fluid cells to allow a continuous injection of gas and water

Two production pumps (3) are connected to the outlet of the core-holder. They represent production wells and allow a continuous production and quantification of the effluents at reservoir conditions (P&T)

A flashing system (back pressure regulator) was set after production pumps. When a pump finished its production, the second one takes over. During the production phase of

the second pump, the first one was emptied and all the fluids from different phases as described in Fig.7 were measured at both reservoir and standard conditions (4).

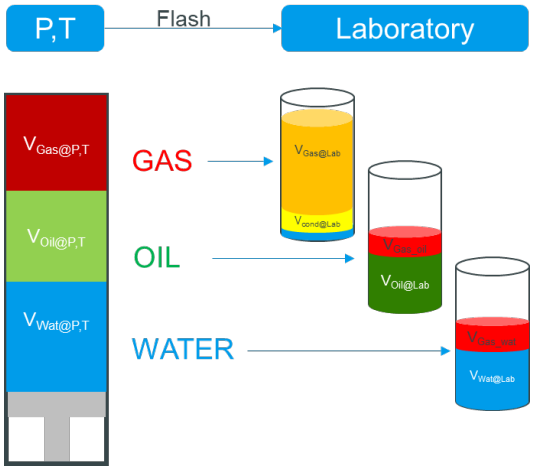

Fig. 7. Reservoir and standard volume process

Gas chromatography (5) was continuously performed during the purge phase of the production system with a gas volume quantification. Oil produced samples were taken during this same phase (4) to a gas chromatography of the liquid phase and evaluate the composition evolution of the produced oil.

Differential pressure (6) was measured continuously during all the core preparation and WAG experiments.

The core-holder was set in an X-Ray monitoring system (described in section 3.5) horizontally for WAG1, WAG2 and WAG3. Our patented X-Ray system called CXBox renders the flexibility to install the core-holder vertically for WAG1b.

3.2 Core preparation

Cores samples were first cleaned and then dried by the injection of solvents and nitrogen, respectively. They were characterized with solvent miscible tracer test to assess the homogeneity of the sample, then undergone helium porosity, gas permeability measurement. Finally, they were filled with water to determine the water permeability value (as reference permeability).

The best three candidates were selected to follow the reservoir conditions process closely as described by Duchenne et al. [10].
Cores were set back to reservoir conditions using the following procedure:

1) Load the core holding cell horizontally on the X-Ray test stand. Set a 50bar confining pressure in the annulus.
2) Fill core with 100% nitrogen content. Measure permeability to gas.
3) Create vacuum inside the core. Perform X-Ray dry counting.
4) Fill the core with 100% brine. Measure permeability to formation water. Use the volume balance to calculate pore volume (PV) and porosity. Perform X-Ray 100% brine image acquisition.
5) Primary drainage: inject synthetic mineral oil, increasing rates step by step and reversing direction of injection until initial water saturation (Swi) targeted is reached. Perform X-Ray Swi image acquisition at laboratory conditions.
6) Increase temperature and pressure to reach experimental conditions, while maintaining confining pressure 50 bars above experimental pressure. Replace synthetic oil with crude oil using a buffer of toluene.
7) Ageing process: maintain the core at reservoir conditions for two weeks to restore rock wettability with oil under flooding or submerging. Measure permeability to crude oil after ageing. Perform X-Ray Swi image acquisition at reservoir conditions.
8) Replace crude oil by reservoir live oil and measure permeability to live oil after ageing. Perform X-Ray Swi image acquisition at reservoir conditions.

3.3 Corefloods

The design of high pressure and high temperature experiments was performed using 1D simulation based on simplified conditions (10 bars and 90°C) experiments:

- W/O/W/O: Alternating injection of water and oil to study the displacement of water by oil that occurs in the reservoir when an oil bank is mobilized by gas injection after an initial water sweep. The core was set to Swi and the water/oil viscosity ratio was maintained.
- G/O/G/O: Alternating injection of gas and oil to study the displacement of gas by oil and to determine the associated hysteresis parameters. The gas was nitrogen.

Two phase relative permeabilities G/O and W/O were defined based on these experiments and were implemented on a 1D compositional simulation core model.
The first flow rate considered was 15 cc/h for water and gas, which corresponds to a front speed of 3 ft/day in the field.
The injected water was formation water, see section 2.4, and the injected gas is described in section 2.5.

Long slug injections WAG1a
The first experiment consisted of alternating four long slugs of gas and water: G1 – W2 – G3 – W4. Each gas injection phase followed the same protocol: start injection at 15 cm^3/h and wait for stabilization in production and pressure drop (i.e., no more saturation changes after several pore volumes injected); raise injection rate to 30 cm^3/h until steady state is reached and then to 75 cm^3/h so as to reduce capillary end effects; finally return to initial injection rate, by decreasing rates step by step. For the water injection phase, the flow rates applied were 15 cm3/h, 30 cm3/h, 60 cm3/h and 100

cm3/h. WAG1 ended with a final chase water injection to evaluate the trapped gas.

Long slug injections WAG1b
The second experiment was the same as WAG1a but with a vertical core sample setup. All fluids were injected into the top of the core to ensure a gravity stable gas injection. The reservoir is too flat (dip ~1°) for gravity segregated flow to be applicable in the field. Therefore, this experiment is only a theoretical verification of the gravity impact on the results. Skauge et al. [11] studied the Kr dependance on core orientation.

Long slug injections WAG2
The third experiment consisted of alternating four long slugs of water and gas: W1 – G2 – W3 – G4. Protocol was the same as WAG1. Flow rates had to be changed because of the higher permeability. To be sure to obtain a differential pressure consistent and measurable, we had to increase them to 20 cm3/h, 60 cm3/h and 100 cm3/h for W1, G2, W3. A flow rate at 30 cm3/h was added for G4 and finalized by a chase gas to determine the trapped water.

Short slug injections WAG3
The last experiment was carried out by conducting a 10-cycle injection sequence of alternating short slugs (0.125 PV) of gas and brine, starting with gas. The flow rate was set at 15 cm3/h. A last injection of gas was conducted as chase gas to have another value of trapped water (as in WAG2) with a sequence of flow rates of 15, 30, 60 and 100 cm3/h.

3.4 Material balance calculations

All data acquisitions during the injection and production phase, especially volumes are presented in Fig.7. Recovery factors and fluid saturations can be determined using different methods hence different values are obtained as described below:

Recovery factors:

The first way to calculate oil recovery factor is to consider the oil volume produced at reservoir conditions ($V_{Oil@P,T}$) and the volume of oil produced from the gas phase after flash. For this condensate or light oil produced by the gas, it is considered that the ratio of volume at reservoir condition and lab condition (Bc) is different than Bo. The reference volume in this case is the initial oil volume at reservoir conditions (HCPV):

$$RF_{downhole.corrected} = \frac{(V_{Oil@P,T} + Bc * V_{cond@Lab})}{HCPV} \quad (1)$$

With: $HCPV = Vp * (1 - Swi)$

Using the same oil volume produced at P&T, the oil recovery factor can only consider the volume of oil produced during the oil purge and neglect the oil produced by gas phase:

$$RF_{downhole.direct.w/oCond} = \frac{V_{Oil@P,T}}{HCPV} \quad (2)$$

Our experimental setup allows us to measure the volume of oil produced both at reservoir conditions and at laboratory conditions. Lab volume produced can be used for the oil recovery factor considering the oil volume produced at laboratory conditions ($V_{Oil@lab}$) and the oil produced with the gas phase ($V_{cond@Lab}$). The reference volume is the initial volume of oil at laboratory conditions (STOOIP). In this case, condensate is counted as oil ($Bc = Bo_i$):

$$RF_{surface.direct} = \frac{(V_{Oil@Lab} + V_{cond@Lab})}{STOOIP} \quad (3)$$

In the same philosophy as equation (2), we can only consider the oil volume produced in laboratory conditions and do not consider condensate:

$$RF_{surface_{w/oCond}} = \frac{(V_{Oil@Lab})}{STOOIP} \quad (4)$$

With: $STOOIP = {}^{HCPV}/_{Bo_i}$

The last way to calculate the oil recovery factor is in the same approach as equation (3) but here, Bc is considered different than Bo and must be determined using our internal fluid simulation software BEST:

$$RF_{surface_{cond.corrected}} = \frac{\left(V_{Oil@Lab} + {}^{Bc}/_{Bo_i} * V_{cond@Lab}\right)}{STOOIP} \quad (5)$$

In the case of strictly immiscible and incompressible conditions, the five methods should yield the same results (within measurement uncertainty).

In this study, multi-contact miscible exchanges were expected (and desired) between gas and oil as shown on Fig.4. Therefore, the different recovery factors give complementary information on the swelling (oil volume increasing by gas absorption) and stripping (extraction and transport of light oil components by gas) concept.

The difference between equation (2) and equation (4) represents the impact of swelling. In equation (2), reservoir oil volumes are overestimated (gas absorption) and in case of huge exchange recovery can reach values higher than one.

The difference between equation (3) and equation (4) depends on stripping and represents the impact of the light oil produced by the gas phase on the oil recovery.

These 2 concepts are illustrated using Fig.9 in the results chapter.

Fluid saturations:
From previous recovery factors calculation, the same number of oil saturation results can be considered with the

same assumptions and introducing the notion of initial oil saturation (Soi):

$$So_{downhole\_corrected} = Soi \cdot (1 - RF_{downhole\_corrected}) \quad (6)$$

$$So_{downhole\_direct\_w/oCond.} = Soi \cdot (1 - RF_{downhole\_direct\_w/oCond.}) \quad (7)$$

$$So_{surface\_direct} = Soi \cdot (1 - RF_{surface\_direct}) \quad (8)$$

$$So_{surface\_w/oCond.} = Soi \cdot (1 - RF_{surface\_w/oCond.}) \quad (9)$$

$$So_{surface\_cond.\ corrected} = Soi \cdot (1 - RF_{surface\_cond.\ corrected}) \quad (10)$$

Water saturation is simpler to deduce. It is necessary to consider the initial/irreducible water saturation obtained during the drainage phase, then the cumulated injected and produced volumes of brine at reservoir conditions, $V_{injw(P,T)}$, $V_{prodw(P,T)}$ respectively.

$$Sw = Swi + (V_{injw@P,T} - V_{prodw@P,T}) / PV \quad (11)$$

Gas saturation is calculated using the closing equation (12). Note that the closing equation is made on gas because produced water volumes are usually more reliable than produced gas volumes.

$$Sg = 1 - So - Sw \quad (12)$$

Fluid analysis:

Main characteristics of fluid evolution during time can be calculated for a perfect understanding of the exchange between gas and oil and its impact:

$$Bo = V_{Oil@P,T} / V_{Oil@Lab} \quad (13)$$

$$Rs = V_{Gas\_oil} / V_{Oil@Lab} \quad (14)$$

$$GOR = (V_{Gas@Lab} + V_{Gas\_oil}) / (V_{Oil@Lab} + V_{Cond@Lab}) \quad (15)$$

$$Bg' = V_{Gas@P,T} / V_{Gas@Lab} \quad (16)$$

3.5 2D imaging system monitoring

Setup description

2D X-ray cabinet called CXBOX (Fig.8) was used for this study. As described by Savin et al. [12], this tool features the following components:

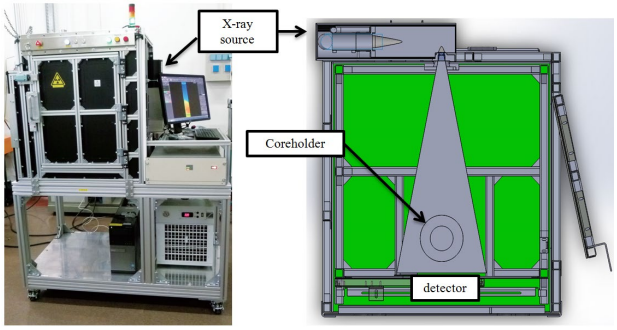

Fig. 8. Photo and diagram (top view) of the CXBOX1 2D bench after development

X-ray source: Multiple designs with varying power ranges (from 50 to 500W) were developed to accommodate different applications, particularly based on the reservoir core size. In the case of this program with a core diameter of 50 mm, the generator is set to 120 kV and 1.8 mA. These X-ray generators are designed to operate continuously for several weeks while maintaining high stability, with dose fluctuations remaining below 0.5% over at least 24 hours.

Flat panel detector: Utilizing amorphous silicon and Gadox scintillator technology, the detector has an active area of 40 cm by 40 cm and a pixel size of 200 µm.
The coreholder is positioned as close to the detector as possible, maintaining a minimum distance of 50 cm from the X-ray generator.

Saturation calculation methods

The flat-panel detector produces grayscale images that represent the 2D projection of the entire rock. From these images, two methods were developed and tested for fluid visualization and saturation calculation: the linear method and the Beer-Lambert law method. The latter method was employed in this study.

Calculation method 2: using the Beer-Lambert law

This method involves extracting information from the received dose (N), which is displayed in grayscale within a predetermined area (a pixel, a pixel line, or the entire rock sample). The saturation of this area is then determined by applying the Beer-Lambert law. Standard pieces allow for continuous monitoring of changes in fluid attenuation coefficients within the injection or production circuit, enabling adaptation of interpretation and calculation to accommodate variations in fluid composition. Fluid saturation is calculated using the Beer-Lambert law by comparing the difference in fluid saturation between two states (two images). Equation 18 demonstrates the calculation of oil saturation (So) during waterflooding after achieving irreducible water saturation (Swi); in this instance, the Swi image (N_{swi}) serves as the reference. The attenuation coefficients of the injected water (µ_water) and reservoir oil (µ_oil) are derived from the standard. According to the Beer-Lambert law, we obtain:

$$So = So_{swi} + \frac{\ln\left(N_{current\_image} / N_{swi}\right)}{\emptyset * l * (\mu_{oil} - \mu_{water})} \quad (18)$$

With $\emptyset$ = local porosity.

The calculated saturations can then be averaged and depicted in a graph. One of the key advantages of this setup is that it allows for fluid saturation of the rock to be determined independently from the material balance.

Pseudo-2phases method

Due to the presence of three phases (gas, oil, and water) during WAG experiments, the traditional saturation

calculation method only determines the saturation of two phases. To obtain information on the third phase, a second energy level must be generated as described by Caubit et al.[13]. This is feasible with our system but requires a high-frequency acquisition rate. In our study, we aimed to clearly track the fluid path, particularly that of the gas. Therefore, we considered only two phases during gas injections: a gas phase and a liquid phase. The attenuation coefficient (μmix) for the mixture is calculated using the following equation:

$$\mu mix = \mu wat * Swat + \mu oil * Soil / (Swat + Soil) \quad (20)$$

The same assumption can be applied to observe the variations in injected fluid saturation during subsequent stages.

4 Results and discussion

4.1 Long slugs horizontal WAG1 (G-W-G-W)

Oil recovery factors reflect high sweep efficiency by gas in two-phase flow and even better in three-phase flow. Strong swelling and huge striping were observed during this experiment as shown on Fig.9.

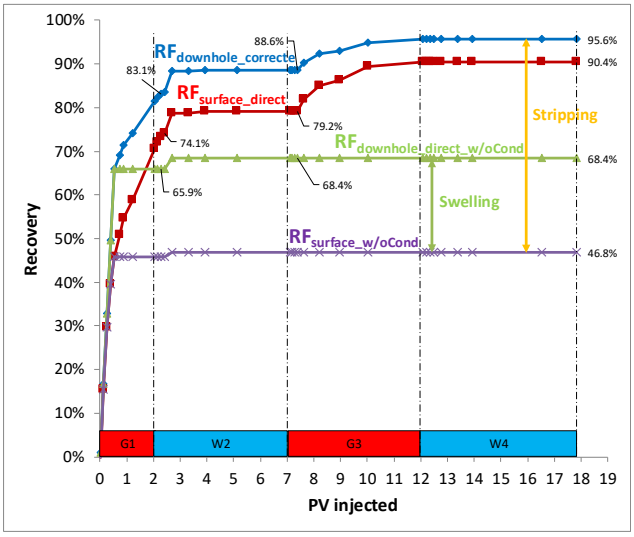

Fig.9. Oil recovery factors calculated for WAG1a

The analysis of saturation graph highlights trapped saturation gas (Sg_trapped) increase depending on the cycle (W2 vs W4). Differential pressure during G3 was four times higher than during G1 due to gas cycling reduction. It is positive for the secondary drainage parameters used on reservoir simulation model.

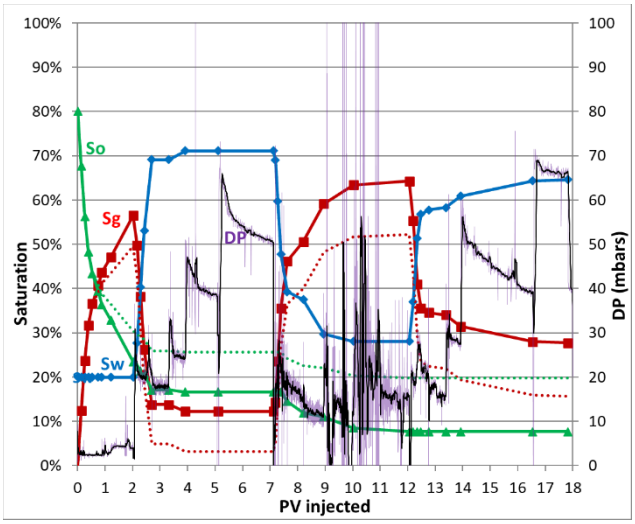

Fig. 10. Oil, gas, water saturations and differential pression versus number of pore volumes injected during WAG1a experiment

CXBox interpretation shows a huge gravity effect (Fig. 11). The gas path is clearly guided on the top of the core sample with a progressive desaturation to the middle of the porous medium. However, the bottom part of the core left non-contacted by the gas.

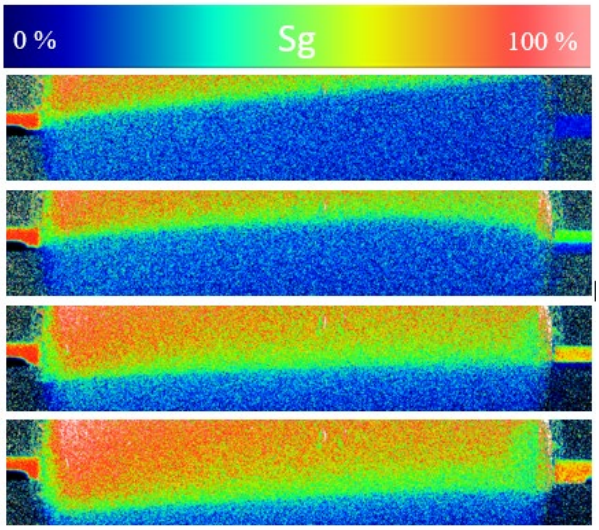

Fig.11. Gas saturation observed at 0.16, 0.3, 0.9 and 2 PV of injected gas using CXBox tools during first gas injection of WAG1a. Gas injection from left to right. Clear gravity impact with gas path on the top of the core.

During water injection (Fig.12), the non-invaded by gas area was desaturated by injected water. High gas between gas and water was observed.

Fig.11 and Fig.12 demonstrate clearly the positive impact of injected fluids with density differences in high permeability core where gravity has a significant impact on the sweep behaviour.

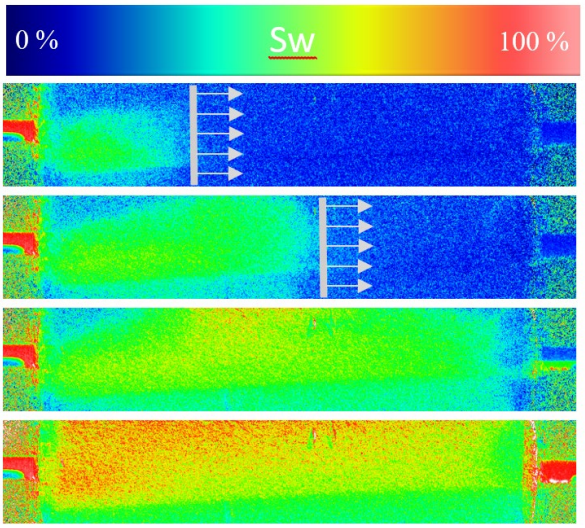

Fig.12. Water saturation observed at 0.16, 0.3, 0.4 and 7 PV of injected water using CXBox tools during first water injection of WAG1a. Water injection from left to right. Desaturation of the non-contacted by gas area.

The second gas injection (Fig.13) demonstrates another advantage of cycling gas and water injections. The gas front was clearly stabilized by the presence of water. Areas initially non-contacted by gas can benefit gas-oil interaction and increase oil production by swelling and striping.

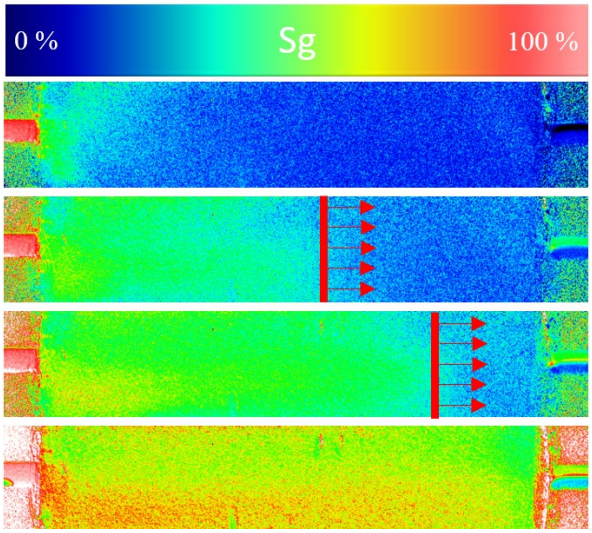

Fig. 13. Gas saturation observed at 2.2, 2.4, 2.6 and 7 PV of injected gas using CXBox tools during second gas injection of WAG1a. Gas injection from left to right. Clear stabilization of the gas front.

Gas-oil interaction is clearly observed in the analysis of the oil effluent samples measured by chromatography (Fig.14). Masalmeh S. et al [14] showed a similar observation. Light components proportion reduced during the successive production purges. As shown by Wanat et al. [15], it is due to the stripping effect with the light component which are transported by gas. It is completely the opposite for the intermediate components. Less and less light component means a higher proportion of heavier ones. The heaviest components seem to be stable.

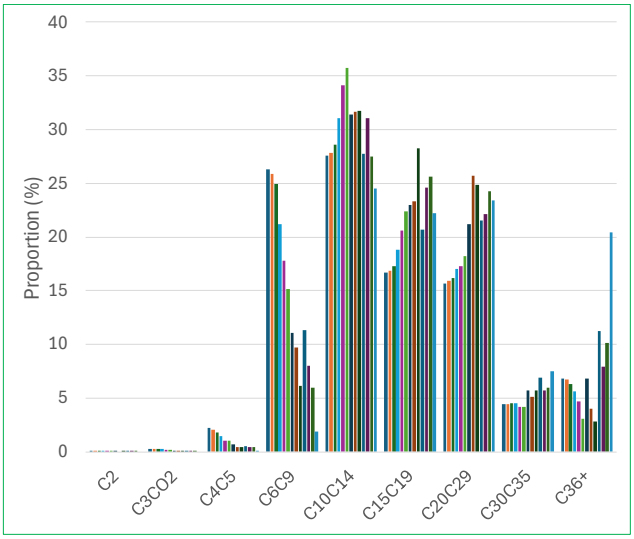

Fig. 14. Evolution of produced oil composition purges after purges measured by chromatography.

4.2 Long slug vertical WAG1bis (G-W-G-W)

When gas sweep is stabilized by gravity, the vertical WAG experiment showed great efficiency of gas injection. The entire volume of oil was produced by the first gas injection. Moderate stripping and no swelling were observed (Fig.16) due to the low and stabilized contact surface of gas and oil (Fig.15).

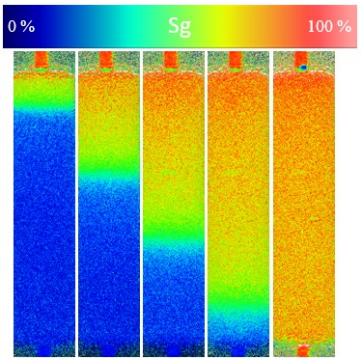

Fig. 15. Gas saturation observed at 0.03, 0.17, 0.44, 0.6 and 2.7 PV of injected gas using CXBox tools during first gas injection of WAG1b. Gas injection from top to bottom. Gravity stabilized gas front.

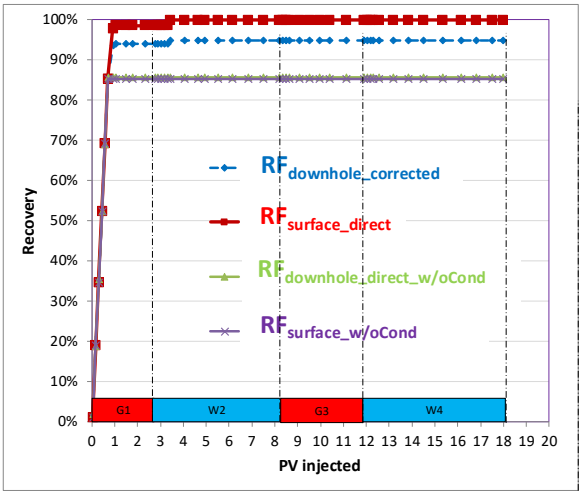

Fig. 16. Oil recovery factors calculated for WAG1b (vertical injections Top - Bottom)

4.3 Long slugs WAG2 (W-G-W-G)

The first water injection in this experiment shows low oil recovery efficiency. Despite the presence of water, the subsequent gas injections yield good oil production efficiency (three-phasic phases).
Stripping is moderate compared to WAG1 experiment and no swelling was observed.

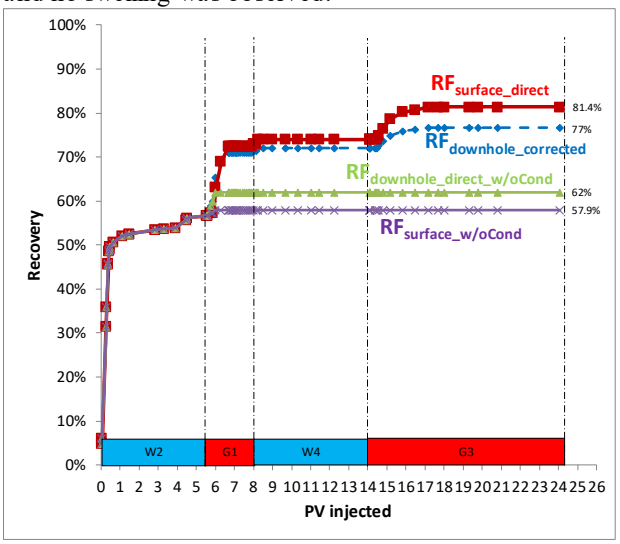

Fig. 17. Oil recovery factors calculated for WAG2

The first water injection corresponds to a two-phase coreflood. CXbox interpretation can be included in the calculation of the oil saturation changes versus time.
Gravity effect was observed with an unbalanced velocity front to the bottom of the porous medium. Fig.18 shows the decrease of oil saturation:

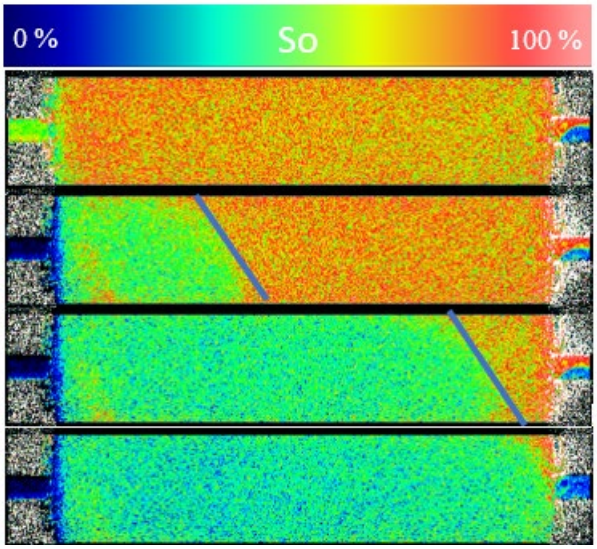

Fig. 18. Oil saturation observed at 0, 0.04, 0.27 and 5.6 PV of injected water with CXBox tools during first water injection of WAG2. Water injection from left to right.

Another way to interpret CXBox images is to calculate the gas saturation whatever the injection phase (Fig.19 - 21). The gas front was stabilized only on the last gas injection. The impact of the difference in density was observed during the first gas injection and the second water injection.

The trapped gas can also be observed at the end of the second waterflood (Fig.20).

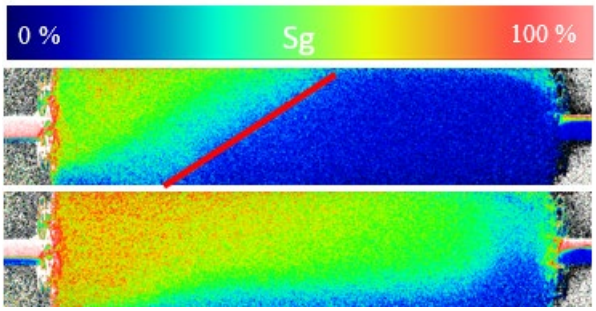

Fig. 19. *Gas saturation at 5.9 and 7.9 PV of gas injected from the G2 three-phasic phase of WAG2. Gas injection from left to right*

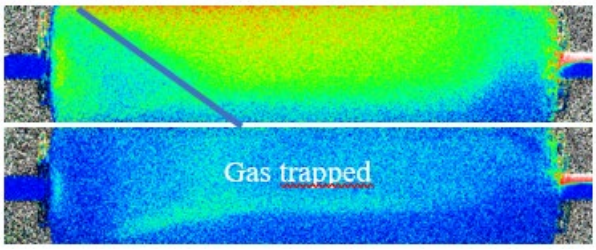

Fig. 20. Gas saturation at 5.47 and 11.8 PV of injected water from the W3 three-phasic phase of WAG2. Water injection from left to right

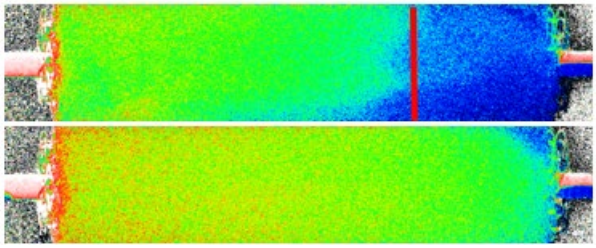

Fig. 21. Gas saturation at 8.3 and 17.9 PV of injected gas from the G4 three-phasic phase of WAG2. Gas injection from left to right.

4.4 Short slugs WAG3

Short slugs experiment is the most representative of the field process with slugs size designed to be consistent with the ones at field scale.

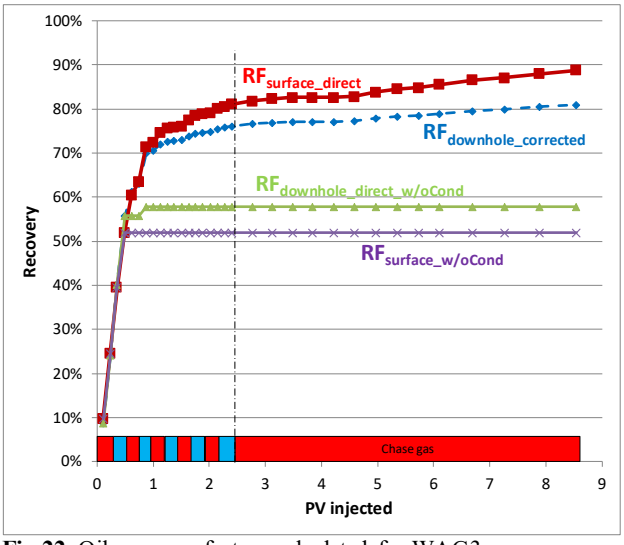

Fig 22. Oil recovery factors calculated for WAG3

This experiment demonstrated significant gas and total sweep efficiency leading to a very high recovery factor of 95% (Fig.22). The stripping was large, and the swelling was considered as moderate compared to WAG1 (high swelling) and WAG2 (no swelling).

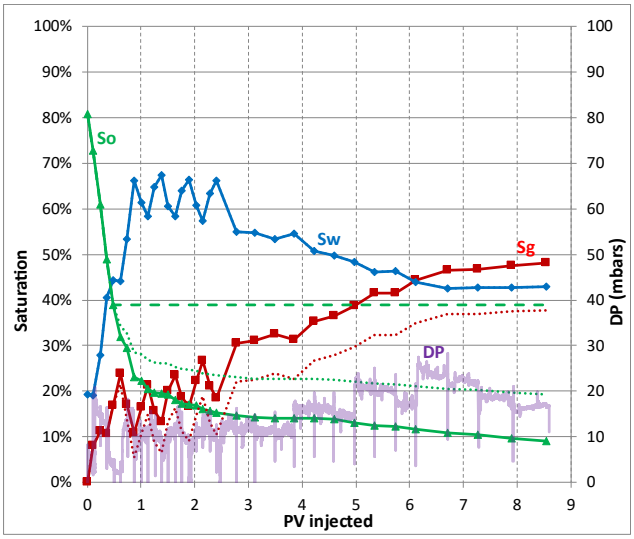

Fig. 23. Oil, gas, water saturations and differential pression versus throughput during WAG3 experiment.

Differential pressure was quite stable on cycling mode (Fig.23), where just two cycles gas-water was applied to reach stabilization.

4.5 Experiments comparison

A good way to compare the full program is to plot the saturations evolution on a ternary diagram (Fig.24). It allows to track the three saturations simultaneously, and to verify that the KRs are anchored on the complete 3-phase region.

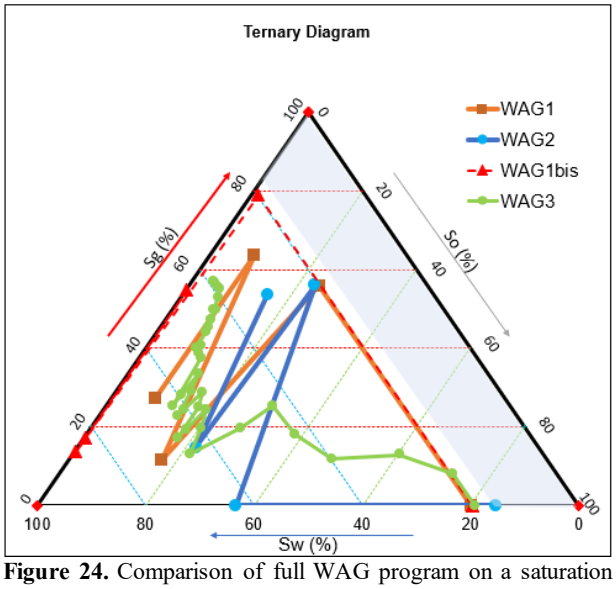

Figure 24. Comparison of full WAG program on a saturation ternary diagram

Figure 24 shows an increase of the remaining gas saturation depending on the cycles. WAG3 confirms that the beneficial synergy between waterflood and gasflood is stronger for short slugs than for long slugs. It has the quickest recovery (area 1 in Fig. 25) of all horizontal displacements. It proves the benefit of three-phase flows with a good correlation of all advantages of WAG experiment: sweeping of different areas (density of fluid and gravity) and gas-oil interactions (stripping and swelling).

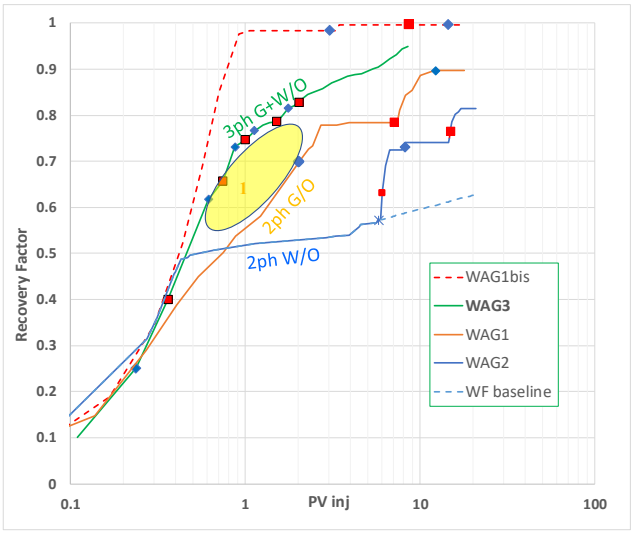

Fig. 25. Oil recovery comparison for the full program

5 Conclusion

This paper presented a state-of the-art experimental WAG data set, and the design and methodology used to acquire it, in multi-contact miscible conditions representative of the field. Advanced monitoring was used for the 3 saturations (in 2-D and 1-D), and for the compositions, allowing to calibrate gas-oil interaction and to distinguish its effects from petrophysical changes (typically KR evolution in 2-phase and 3-phase).

In the WAG1 experiment, high sweep efficiency was achieved with strong swelling and stripping effects. The experiment noted increased trapped gas saturation and enhanced gas desaturation, facilitated by gravity and favorable viscosity ratios. Cycling gas and water injections stabilized the gas front, thus boosting oil production.

The WAG2 experiment showed low waterflood efficiency compared to a highly efficient gasflood in three-phase flow. Moderate stripping was observed without swelling. CXBox equipment was useful for tracking oil and gas saturation, and density differences impacted injections, with trapped gas noted.

The WAG3 experiment, representative of field processes with appropriately scaled slug sizes, demonstrated significant gas and total sweep efficiency, leading to a very high recovery factor of 95%. The stripping effect was large, while the swelling was moderate, in contrast to WAG1 (high swelling) and WAG2 (no swelling). Differential pressure remained stable during the cycling

mode, with only two gas-water cycles required to reach stabilization.

The WAG1b experiment demonstrated significant gas efficiency when controlled by gravity. The first gas injection successfully produced the entire volume of oil, with moderate stripping and no swelling. A low and stabilized contact surface was observed between gas and oil.

Comparatively, short slugs in WAG systems provided quicker recovery in horizontal displacements, highlighting the benefits of three-phase flows, including efficient sweeping and gas-oil interactions.

Nomenclature

Bc = condensate formation volume factor

Bg = gas formation volume factor

Boi = initial oil formation volume factor

BSW = basic sediments and water

EOS = fluid equation of state

GOR = gas oil ratio

HCPV = hydrocarbon pore volume

Kg, Kl = gas permeability, Klinkenberg corrected

Kw = water permeability

MMP = minimum miscibility pressure

Mw = molecular weight

RF = recovery factor

Rs = solution gas

SCAL = special core analysis

STOOIP = stack tank original oil in place

Swi = irreducible water saturation

WAG = water alternating gas

References

1. Bourgeois, M. : « Recent Importance of Gas-based EOR", EAGE 2025, https://doi.org/10.3997/2214-4609.2025101529
2. Pizarro, J. O. S., et al: "Optimizing Production of Santos Basin Pre-Salt Fields through Sound Reservoir Management Practices", OTC-27993, 2017.
3. Shahverdi H., Sohrabi M.: "An Improved Three-Phase Relative Permeability and Hysteresis Model for the Simulation of a Water-Alternating-Gas Injection", SPE-152218, 2013
4. Burns, L., et al.: „Guyana: Liza Phase 2 Novel Execution to Accelerate Field Development", OTC-30948, 2021.
5. Joubert, T. , Duchenne, S., Bourgeois, M., de Loubens, R., and Petitfrere, M. : « Experimental Data Acquisition and Modeling for the Study of Miscible CO2 WAG in Carbonate Reservoirs Under Oil-Wet Conditions", SPE-188471, 2017.
6. Vieira, R., Cardoso, M. A., Pizarro, J. O. S.: "An Integrated WAG Characterization Study for an Offshore Oilfield", OTC-29766, 2019
7. Egermann, P., Robin, M. and Lombard, J.-M.: "Gas Process Displacement Efficiency Comparisons on a Carbonate Reservoir", SPE-81577, 2003.
8. Bourgeois M., Hunter M., Le Goff C., Lindeloff N.: "Investigation of Methodology to Degrade Miscibility in Compositional Simulation", EAGE, 2025; https://doi.org/10.3997/2214-4609.202531054
9. Duchenne S., de Loubens R., Petitfrère M., Joubert T.: "Modeling and Simultaneous History-Matching of Multiple WAG Coreflood Experiments at Reservoir Conditions", SPE-177531, 2015
10. Duchenne S., Puyou G., Cordelier P., Hy-Billiot J., Hamon G.: "Efficient Experimental Data Acquisition for Miscible CO2 WAG Injection Corefloods in Carbonate", SPE-169045, 2014
11. Skauge A., Skauge T., Sorbie K;, Bourgeois M.: "Impact of Viscous Instabilities on WAG Displacement", SPE-211448, 2022
12. Savin S., N'Guyen M., Puyou G.: "CXBOX: An Innovative Tool For Fluid Dynamic Quantification During Corefloods", SCA037, 2017
13. Caubit, C., Bertin, H., and Hamon, G.: "Three-Phase Saturation Measurement During Gravity Drainage and Tertiary Waterflood: Improvement on Dual Energy Gamma-Ray Attenuation Technique", SCA2004-06
14. Masalmeh S., Farzaneh S., Sohrabi M., Alhammadi M.: "Experimental Investigation of Factors Affecting Oil Recovery and Displacement Efficiency of CO2 Injection in Carbonate Reservoirs", SPE-218525, 2023.
15. Wanat, E., Teletzke, G., Newhouse, D., Lawrence, J., Al Shehhi, R., Willingham, T., and Al Jawhari, O.: "Quantification of Oil Recovery Mechanisms during Gas Injection EOR Coreflood Experiments", SPE-188691, 2017.